Carbon dioxide reforming of methane over Ni-In/SiO_2 catalyst without coke formation

Johanna Károlyi[a], Miklós Németh[a], György Sáfrán[b], Zoltán Schay[a], Anita Horváth[a], Ferenc Somodi[a]*

[a]Hungarian Academy of Sciences, Centre for Energy Research, Institute for Energy Security and Environmental Safety, Department of Surface Chemistry and Catalysis, Konkoly-Thege M. street 29-33, H-1121 Budapest, Hungary
[b]Hungarian Academy of Sciences, Centre for Energy Research, Institute for Technical Physics and Materials Science, Konkoly-Thege M. street 29-33, H-1121 Budapest, Hungary

*corresponding author: somodi.ferenc@energia.mta.hu

Keywords
dry reforming of methane, silica supported nickel catalyst, nickel-indium bimetallic catalyst, coke formation, biogas conversion

Highlights

- Ni-In/SiO_2 catalysts were prepared by deposition-precipitation with urea.
- Both metals were in metallic state after reduction at 700 °C.
- Interaction of the two metals was evidenced by TPR, XPS.
- The presence of indium in the close vicinity of nickel prevents coke formation.

Graphical abstract

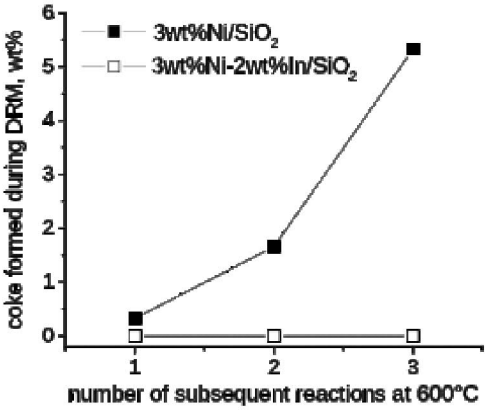

Abstract

The development of a carbon tolerant nickel catalyst for carbon dioxide reforming of methane (dry reforming of methane, DRM) has been in the focus of catalysis research for several years.

In the present study, 3wt%Ni/SiO_2 and bimetallic 3wt%Ni-2wt%In/SiO_2 catalysts (corresponding to 3:1 Ni:In ratio) were prepared by deposition precipitation with urea. Our intention was to modify the nickel surface with a second metal which is known from its ability to reduce surface coke formation. A methane rich reaction mixture (CH_4:CO_2:Ar =

69:30:1) was used for the catalytic tests at 600 °C and 675 °C. TPO measurements after the catalytic tests showed that there was no surface carbon formation on the indium containing catalyst.

Temperature-programmed reduction measurements of the catalysts showed that both nickel and indium was completely reduced after one hour reduction at 700 °C suggesting interaction of the two metals. CO pulse chemisorption experiments revealed that the particle size was similar on the monometallic and bimetallic catalyst, and CO-TPD measurements showed completely different desorption behavior of CO, suggesting the presence of different active sites on the two catalysts. XPS experiments gave similar results, furthermore it was found that after reduction, the Ni/In ratio on the surface was 2.2 compared to the initial value (~3), which refers to the surface enrichment of indium in the bimetallic particles.

The lack of coke formation on the indium containing catalyst might be explained by the interplay between a geometric and a chemical effect, that is, indium atoms are most likely situated on the edge and step sites of a nickel particle, influencing reactant adsorption and hindering the growth of carbon nanostructures and/or providing an oxygen rich indium suboxide surface through the reaction with CO_2 in the close vicinity of catalytically active nickel sites, which also inhibits the accumulation of carbon deposits during DRM.

1. Introduction

Utilization of carbon dioxide is one of the biggest challenges of our time, because the vast majority of the anthropogenic CO_2 is emitted to the environment playing significant role in the climate change [1], [2]. A possible pathway is the transformation of carbon dioxide through the synthesis of liquid fuels using renewable or non-hydrocarbon based energy sources during the process [3]. The current opinion is that the reduction of carbon dioxide with methane (dry reforming of methane (DRM) $CO_2 + CH_4 \rightleftharpoons 2\ CO + 2\ H_2$) would be a suitable reaction, since the product is synthesis gas, which is one of the most important feedstock of chemical industry, Fischer-Tropsch synthesis is used for the production of liquid fuels [4], [5], [6].

The reaction of carbon dioxide with methane is endotherm, high temperature is necessary to reach the desired conversion. Although noble metals (e.g.: Ru, Rh, Pt, Pd) show high conversion and slow deactivation rates and minimal coke formation [3], [7], [8], [9], use of nickel catalyst would be more feasible because of its lower price and higher abundance. Unfortunately, carbon deposits more readily form on nickel than on noble metal surfaces during the reaction leading to fast deactivation of the catalyst [10].

The side reactions responsible for the surface carbon formation during DRM are the methane decomposition and the carbon monoxide disproportionation (Boudouard reaction) [11]. These reactions occur in wide temperature ranges (the former is endothermic and the latter is exothermic), that is, carbon formation on nickel surfaces is thermodynamically favorable, unless the reaction is carried out at temperatures above 800 °C with high CO_2/CH_4 feed ratios [11].

Besides the reaction conditions, the average particle size of nickel (which is basically determined by the properties of the metal-support interface), the composition/structure of the Ni surface are profoundly affecting the carbon formation on supported nickel catalysts.

Formation of carbon nanofibers, a typical form of surface carbon on nickel nanoparticles during methane decomposition, is structure sensitive [12], therefore small nickel particles are required to minimize coke formation. Accordingly, minimal amount of carbon during DRM was observed on Ni/Al_2O_3 catalysts when the average particle size of nickel was smaller than 7-10 nm [13] [14]. It is quite difficult to maintain the small average particle size under reaction conditions, but it can be achieved by special preparation methods such as

decomposition of nickel precursor by dielectric-barrier discharge plasma over silica [15], molecular layer deposition of porous alumina onto the surface of the catalyst [16] or by preparing porous silica shell around nickel nanoparticles [17].

As it was mentioned above, the properties of the metal support interface has tremendous effect not only on the stabilization of nickel particles, but also on the reactant adsorption and therefore on the tendency of coke formation. Significantly lower amount of coke was observed on Ni/TiO_2 than on Ni/SiO_2 and Ni/Al_2O_3 catalysts during DRM, which was attributed to strong metal support interactions, that is the migration of TiO_x onto the nickel surface. This effect was also responsible for the low catalytic activity of the titania supported catalyst [18].

Basic metal oxide additives modify the metal support interface and participate in carbon dioxide adsorption/activation, which increases the active oxygen concentration around or on the nickel surface leading to decreased carbon formation in DRM [19]. Similarly, the higher carbon tolerance of gallium containing silica supported nickel catalysts compared to Ni/SiO_2 was explained by the gallium oxide induced activated adsorption of CO_2 in the form of carbonate and bicarbonate species [20].

Reducible oxides, such as cerium oxide, take part in the reaction by their active oxygen and might be responsible for the stabilization of the nickel nanoparticles which also leads to decreased coke formation compared to non-promoted catalysts [21].

Instead of adding promoters to the support or using the above mentioned oxides as support materials, modification of the nickel surface sites with other elements has been successfully applied to develop catalysts that are less prone to coke formation. It is generally accepted that highly reactive monoatomic carbon, derived from either dissociative adsorption of carbon monoxide or methane in the case of DRM, diffuses into or polymerizes on the surface of the nickel particles, forming carbon nanotubes or encapsulating carbon, respectively. The presence of another element (metal or non-metal) in the close vicinity of the catalytically active nickel sites may inhibit the polymerization or the diffusion of monoatomic carbon into the particles or might as well promote the gasification reaction of the surface coke [22],[23],[10]. The other element can be alloyed with nickel or it can be present as a physisorbed surface additive. For instance, decreased dissociation of CO was observed on Ni-Cu alloys compared to pure nickel [24], [25]. Carbon monoxide adsorption was inhibited on a nickel (111) surface partially covered by sulfur [26].

The presence of other noble metals, which are themselves inactive in this reaction, was reported to be beneficial to minimize surface coke formation. Silver on Ni/Al_2O_3 catalyst altered the superficial structure of nickel which lead to negligible carbon formation during DRM [27]. Similar behavior was experienced when Ni-Au bimetallic nanoparticles were deposited onto $MgAl_2O_4$: the amount of deactivating carbon decreased during dry reforming [28]. In accord with these findings, it was shown that potassium, sulfur and gold additives preferentially bound to the step sites of the nickel surface which resulted in increased carbon tolerance of these catalysts in steam reforming of methane [29].

Other non-metal elements, such as boron as an additive to nickel was also found to be an effective promoter to suppress surface coke formation [30]. It was suggested based on ab initio DFT calculations, that boron occupies the octahedral sites in the first subsurface layer of the nickel, which prevents carbon diffusion into the bulk of the nickel phase, thereby inhibiting the formation of carbon fibers [31].

Although post transition metals (Ga, Sn, In) are known promoters of supported noble metal catalysts, there is a lack of studies in the literature investigating the role of these metals on supported nickel catalysts in methane reforming reactions. Tin containing yttria-stabilized zirconia supported nickel catalyst showed outstanding stability in steam reforming of methane which was explained by the decreased carbon formation due to enrichment of tin on the

surface of nickel particles [32]. Selective modification of nickel surface on Ni/α-Al_2O_3 catalyst by grafting tetrabutyltin and its subsequent reduction resulted in higher stability and negligible carbon formation compared to the unmodified catalyst [33]. It is worth mentioning that catalysts prepared by co-impregnation had the same properties, that is a coke-free operation without the loss of catalytic activity was observed in the presence of small amount of tin on the catalyst [34].

The goal of our research is to increase coke tolerance of supported nickel catalysts by adding metal promoters to the catalytically active nickel phase. Indium was chosen as a second metal because of its similar properties to tin, and based on its ability to suppress coke formation on platinum catalysts used in dehydrogenation of light alkenes [35]. Silica was used as support material because CO_2 activation is limited on this inert support material, and in the same time allows high degree of nickel reduction [36]. The catalysts were tested in a methane rich gas mixture (CH_4:CO_2 ~ 2:1) modelling the composition of biogas.

2. Experimental

2.1.Catalyst preparation

Monometallic nickel, monometallic indium and bimetallic nickel-indium catalysts were prepared by deposition-precipitation method. Silica support (0.5 g; Aldrich, Davisil, ~300 m^2/g) and urea (2.55 g) were suspended in water under stirring at room temperature until urea was dissolved. Then the precursor solution (nickel(II)nitrate (0.081 M), indium(III)chloride (0.081 M) or both) was added and the mixture was stirred for 3 hours at 80 °C (final pH: 7.5-9). After cooling to room temperature, the powder was separated by centrifugation and washed with Millipore water three times. The products were air dried in an oven at 80 °C for at least 1 day. The nominal metal loadings were set to 3 wt% nickel for Ni/SiO_2, 2 wt% indium for In/SiO_2 and 3 wt% nickel, 2 wt%, indium for Ni-In/SiO_2.

2.2.Catalyst Characterization

2.2.1. TPR, CO chemisorption and TPD

Catalyst characterization was carried out using an AutoChem 2920 Automated Catalyst Characterization System equipped with a TCD detector and a ThermoStar quadrupol mass spectrometer. First, the sample (0.050 g) was calcined in 10% O_2/He flow at 700 °C for 1 hour, then temperature-programmed reduction (TPR) was carried out in 10% H_2/Ar flow up until 700 °C and the temperature was maintained for 1h. The sample was cooled in Ar flow and CO pulse chemisorption was done at 20 °C, with 10% CO/He gas mixture. This was followed by a temperature-programmed desorption (TPD) in He flow until 700 °C which temperature was held for 10 minutes. The desorbed gases were analyzed by a quadrupol mass spectrometer. After cooling down to room temperature this whole charahcterization sequence was repeated two more times. The flow rate of the applied gas mixtures was 50 cm^3/min and the heating rate was 10 °C/min throughout the experiments.

Irreversible adsorption of 1 CO molecule per surface nickel atom was assumed for the calculation of metal dispersion and particle size form the CO pulse chemisorption data.

The results derived from TPR and CO chemisorption are listed in **Table 1**.

2.2.2. X-ray photoelectron spectroscopy

For the determination of surface composition and oxidation state of the metals, X-ray photoelectron spectroscopy (XPS) measurements were done using a KRATOS XSAM 800 XPS machine equipped with an atmospheric reaction chamber. Al K_α characteristic X-ray

line, 40 eV pass energy and FAT mode were applied for recording the XPS lines of Ni 2p, O 1s, In 3d, C 1s, Si 2p regions. Si 2p binding energy at 103.5 eV was used as reference for charge compensation. The samples were measured after preparation and after calcination *ex situ* at 700 °C, these two samples were stored under air before the measurements. Samples after the first TPR were exposed to air during transfer to the XPS, therefore these samples were re-reduced *in situ* at 400 °C in hydrogen flow for 30 min in a pretreatment chamber attached to our spectrometer prior to XPS measurements. After this, the samples were oxidized *in situ* in flowing air at 500 °C for 30 min, which was followed by an *in situ* reduction in hydrogen flow at 500 °C for 30 min. (Atmospheric pretreatment chamber connected to the UHV chamber with a load lock gate allowed us to do pretreatments without contacting the sample with air.)

2.2.3. Transmission electron microscopy

The morphology of the catalysts after 24 hours of dry reforming were studied by a JEOL 3010 high resolution transmission electron microscope operating at 300kV. The samples were prepared by drop drying the aqueous suspensions on carbon-coated micro grids.

2.3.Catalytic tests

Three consecutive catalytic cycles were carried out at 600 °C for 2h using CH_4:CO_2:Ar=69:30:1 reactant mixture with 20 ml/min flow rate. One cycle contained a calcination, a reduction, both at 700 °C for 1h, a reaction, followed by a temperature-programmed oxidation (TPO) of the surface carbon species formed on the catalysts during DRM.

The long catalytic tests (24h) were done at 675 °C using the same experimental settings with new catalyst samples, followed by TPO measurements.

The detailed experimental procedure is the following: The catalytic tests (short and stability tests) were done in a fixed-bed plug flow reactor at 1 atm using CH_4:CO_2:Ar = 69:30:1 mixture. Extremely high concentration of methane was set to mimic biogas composition. 30 mg of catalyst along with 100 mg of diluting quartz beads were placed in a tubular quartz reactor where the reactant mixture at a flow rate of 20 ml/min (40 L/h/g_{cat}) was introduced. At the beginning of the short catalytic tests, the as received samples were in situ reduced in 30 ml/min He:H_2:Ar = 89:10:1 stream at 600 ^oC for 60 min, with a temperature ramp of 10^oC/min. After reduction, the sample was purged with He (30 ml/min) while it cooled down to room temperature. Next, the He flow was changed to the reactant gas mixture and temperature was increased to 600°C with 10^oC/min followed by a 2 h hold time.

The long term isothermal stability tests were lasting for 24 hours. For these experiments, a new portion of the as prepared sample was reduced with He:H_2:Ar = 89:10:1 by heating up the catalyst to 700 ^oC with 10 ^oC/min rate and maintaining this temperature for 30 min. Subsequently, the sample was cooled down to 675^oC in 8 min while it was purged with He, then flowing gas was switched to the DRM mixture. A quadrupole Pfeiffer Prisma mass spectrometer was connected via a differentially pumped quartz capillary to the reactor outlet. Due to the reaction stoichiometry - that causes mass flow increase at the outlet of the reactor - argon was used as an internal reference gas for calculation of the outlet mass flows, to determine CO/H_2 ratio as well as methane and carbon dioxide conversion values, after adequate calibration.

The quantitative analysis was based on the following equation:

$$\frac{f_X * I_X}{I_{Ar}} = \frac{F_X}{F_{Ar}}$$

where F_x = gas mass flow rate (x = CH_4, CO_2, CO or H_2)

F_{Ar} = mass flow rate of argon
I_{Ar} = mass signal of argon
I_x = mass signals (x = CH_4^+, CO_2^+, CO^+, H_2^+)
f_x = calibration factor for each individual gas component.

The following mass signals as representatives of the gas components were measured: 2-H_2, 15-CH_4, 28-CO, 44-CO_2. In quantification of mass signal m/e=28 (CO), the actual fragmentation of m/e=44 (CO_2) was taken into account. The error in carbon balance in the effluent was within +/- 5% in all measurements. The relative difference between two repeated catalytic runs was about 5%. Note that sampling was very fast and the linked symbols showing QMS signals in any of the figures are the results of skipping several measured points for the sake of clarity.

Temperature programmed oxidation (TPO) measurements were conducted in the same flow system to detect and measure carbon deposits formed in the DRM reaction. At the end of the short and long catalytic runs, gas flow was switched to He and the system was cooled to room temperature. Then, the samples were oxidized in 30 ml/min O_2:He:Ar = 10:89:1 mixture by heating from ambient temperature to 700 °C at a rate of 10 °C/min followed by a 60 min isothermal hold. CO_2 signal was used for quantification of coke after a calibration procedure.

3. Results and Discussion

First, the catalysts were calcined, then TPR patterns of the monometallic and bimetallic catalysts were recorded. After each TPR measurement, CO pulse chemisorption at room temperature was done followed by temperature-programmed desorption (TPD) of the chemisorbed CO. This sequence of measurements was done three times without removing the catalyst from the sample tube. The purpose of the consecutive measurements was to get information about the reducibility of the metals, stability of particle size and possible surface changes upon repeated oxidation-reduction cycles.

1.1.Consecutive temperature-programmed reduction (TPR)

The results are summarized in Table 1. and in Figure 1. The first TPR curve of both of the monometallic and bimetallic catalyst is different than the subsequent ones. This difference can be explained by the different character of the nickel oxide-silica interaction after the first and the subsequent oxidations. The catalysts were prepared by deposition-precipitation with urea. It was reported that this method resulted in the formation of layered nickel silicate [37], [38]. It was shown by EXAFS measurements that calcination of a layered nickel silicate above 500 °C resulted in the formation of highly dispersed NiO particles. The reduction of these NiO particles was very difficult (competed above 800 °C) which was explained by the strong interaction between these particles and silica support [38]. The suggested form of strong interaction was that the silica phase from the decomposition of the layered silicate remained in the close vicinity of NiO particles, possibly covering them. Our results are in good agreement with these findings. As it can be seen in Figure 1A, reduction of the calcined sample after preparation takes place at higher temperature (see the first TPR), which suggests the high dispersion of NiO in strong interaction with the support. The strong interaction is maintained between the nickel nanoparticles and silica during reduction, confirmed by the lower amount of chemisorbed CO and hence the lower dispersion and larger particle size compared to the values obtained after the second and the third TPR on Ni/SiO_2 catalyst (Table 1). By the subsequent oxidation, the highly dispersed NiO-SiO_2 phase cannot be restored, the dispersion of NiO on the silica surface is lower after the second calcination

and its reduction is reproducible, as the similarity of the second and the third TPR curves shows.

In the presence of indium, the shape of the first TPR pattern differs from that of the monometallic catalyst: only one broad peak can be observed with a maximum at 460 °C, situated 70 °C lower than the main reduction peak of the Ni/SiO_2 catalyst. The reduction of indium containing oxide phase cannot be separated from the reduction of the nickel oxide. Similarly to the highly dispersed NiO phase on the monometallic catalyst, the surface structure obtained after the first calcination cannot be restored by subsequent red-ox cycles either. The shape and position of the second and the third TPR curve of the $Ni\text{-}In/SiO_2$ catalyst are almost exactly the same, peaks corresponding to the separate reduction of NiO and In_2O_3 cannot be seen, which suggests intimate contact between the particles of the two oxides, dispersed on the silica surface. We assume that the single reduction peak represents the reduction of a mixed indium-nickel oxide phase.

The metal loadings of both catalysts calculated from the amount of hydrogen consumed for the reduction of NiO and In_2O_3 are in accord with the nominal metal loadings. Note that the hydrogen consumption measured on bimetallic catalyst is 1.5 times higher than on monometallic catalyst. This corresponds to 3:1 Ni to In ratio based on the equations below and can be attributed to the complete reduction of metal oxides.

$$3\ NiO + 3\ H_2 = 3\ Ni + 3\ H_2O$$

$$0.5\ In_2O_3 + 1.5\ H_2 = In + 1.5\ H_2O$$

(The amount of hydrogen required for the complete reduction of a bimetallic catalyst with 3:1 Ni:In molar ratio is 4.5 mol, 1.5 times higher than the amount required for the reduction of a monometallic catalyst (3 mol) with the identical nickel oxide content.)

Since separate reduction peak related to the reduction of indium oxide was not observed, a $2wt\%In/SiO_2$ sample was prepared. The TPR patterns of this sample can be seen in Figure 1C. The amount of hydrogen required for the reduction of the indium oxide during the repeated oxidation-reduction cycles decreases (4.6, 3.5, 2.9 cm^3/g_{cat}, respectively), which can be explained by the serious aggregation of the metallic indium phase: during the first reduction, the metallic indium, due to its low melting point, aggregates. The second calcination only partially oxidizes the large indium particles, and therefore the hydrogen needed for their reduction is less than it was after the first calcination. These results suggest that without nickel on the surface, indium is unstable against sintering, the In-Si interaction is rather weak. In spite of these observations, the consumed hydrogen during all of the TPR measurements on the bimetallic catalyst was almost constant (see Table 1), which strongly suggests that indium is in bimetallic interaction with nickel.

Table 1. Hydrogen consumption during TPR and the average particle size and dispersion of nickel calculated based on the results of CO pulse chemisorption.

	$3wt\%\ Ni/SiO_2$			$3wt\%Ni\text{-}2wt\%In/SiO_2$		
	1st	2nd	3rd	1st	2nd	3rd
H_2 (cm^3/g)[1]	9.8	10.3	10.5	15.4	15.3	14.7
CO (cm^3/g)	0.4	0.8	0.7	1.3	0.7	0.6
D (%)[2]	4.3	7.1	6.0	11.7	5.8	5.2
d (nm)[2]	23.4	14.3	16.9	8.6	17.5	19.5

[1]: values at standard temperature and pressure (22414 cm^3/mol).
[2]: values calculated from the amount of chemisorbed CO.

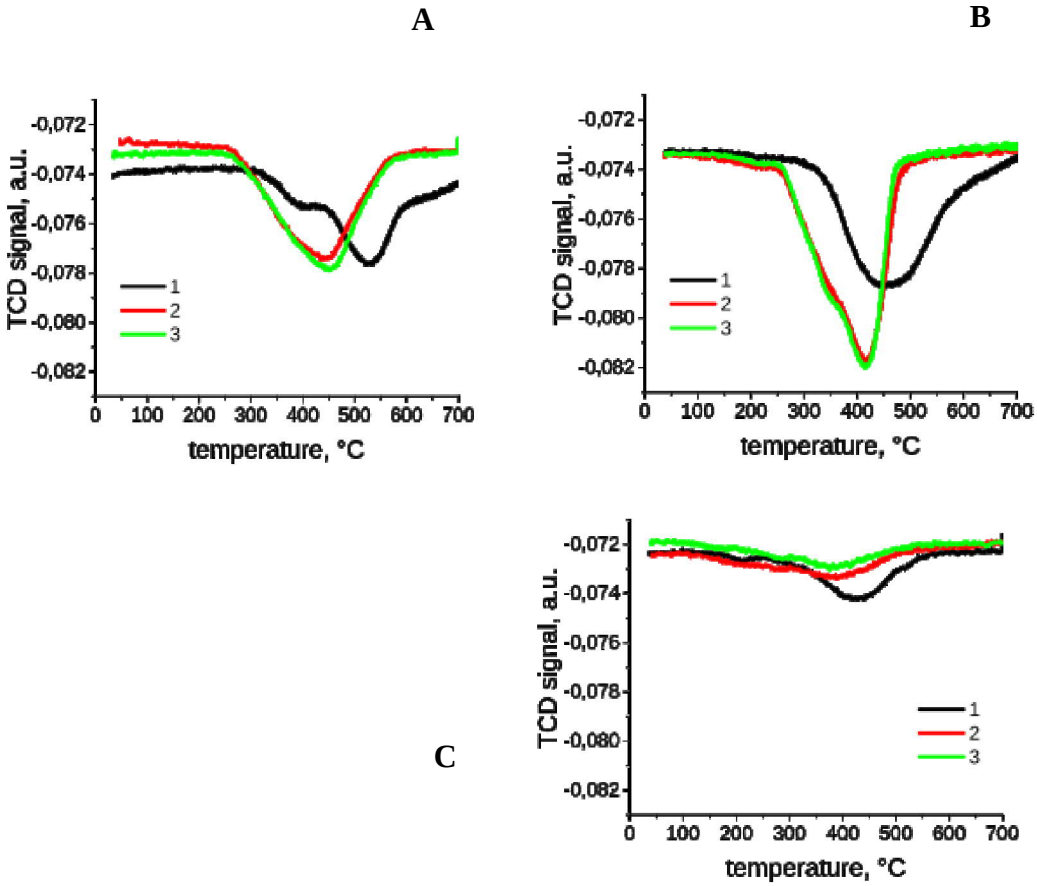

Figure 1. TPR curves obtained during consecutive measurements. Ni/SiO_2 catalyst (A), $Ni-In/SiO_2$ catalyst (B) and In/SiO_2 sample (C).

1.1. Carbon monoxide pulse chemisorption and its temperature-programmed desorption (CO-TPD)

After each TPR, CO pulse chemisorption was applied to get information about the particle size and dispersion of nickel. It can be seen in Table 1 that the particle size slightly increases on both catalysts during the experiments. The results show that the particle size difference between the monometallic and the bimetallic catalyst is insignificant. Note, that nickel carbonyl formation was negligible or below detection limit, since the hydrogen consumption was almost the same during the subsequent TPR measurements, in other words, loss of nickel due to carbonyl formation was not observed after CO pulse chemisorption.

The CO desorption patterns are quite complex, see Figure 2.

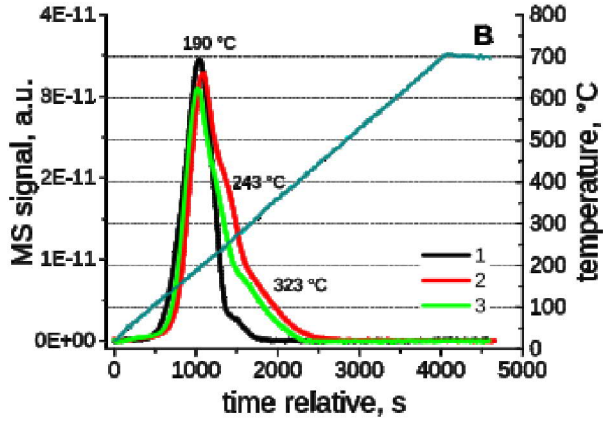
B
190 °C
243 °C
323 °C
1
2
3
MS signal, a.u.
temperature, °C
time relative, s
4E-11
3E-11
2E-11
1E-11
0E+00
800
700
600
500
400
300
200
100
0
0
1000
2000
3000
4000
5000

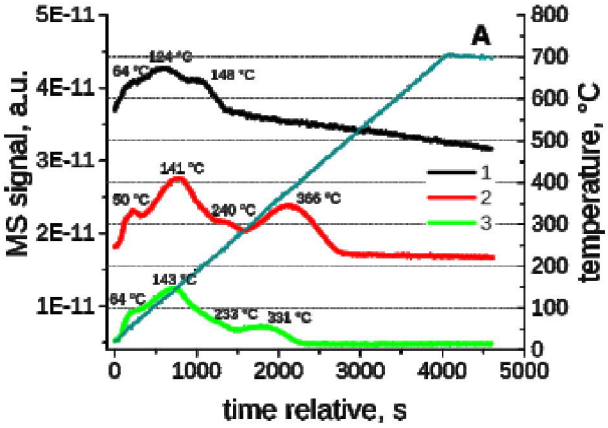
A
64 °C
124 °C
148 °C
50 °C
141 °C
240 °C
366 °C
64 °C
143 °C
232 °C
331 °C
1
2
3
MS signal, a.u.
temperature, °C
time relative, s
5E-11
4E-11
3E-11
2E-11
1E-11
800
700
600
500
400
300
200
100
0
0
1000
2000
3000
4000
5000

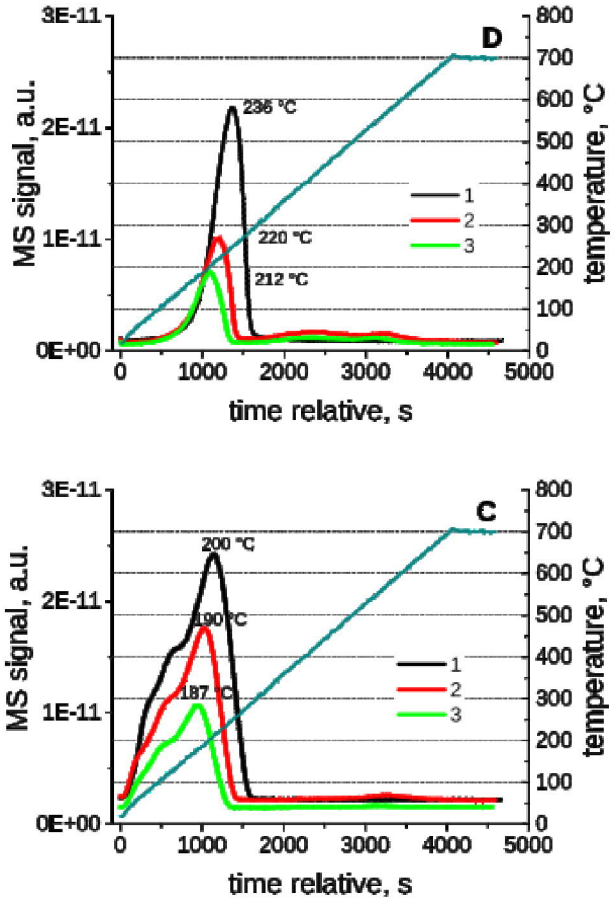

Figure 2. Consecutive CO-TPD patterns (left column) obtained on the catalysts Ni/SiO_2 (A) and $Ni\text{-}In/SiO_2$ (C). CO_2 evolved during the experiments on Ni/SiO_2 (B). CO_2 evolved during the experiments on $Ni\text{-}In/SiO_2$ (D).

Three overlapping CO desorption peak can be seen on Ni/SiO_2 catalyst after the first CO pulse chemisorption, at 64, 124 and 148 °C. After the second and the third oxidation-reduction cycle, three CO desorption peak can be observed as well, however their position is shifted to higher temperatures and a new desorption peak appears above 300 °C. Multiple CO desorption peaks, even higher than 330 °C were observed on silica supported nickel catalysts [39]. It was suggested that CO desorption peaks at low temperature (roughly below 150 °C) were desorption from single site chemisorption and desorption peaks above this temperature

are from two site chemisorption [40], [41]. As it can be seen in Figure 2, high temperature CO desorption peaks above 200 °C are missing in the case of the bimetallic catalyst. This represents the decreased amount of two site CO chemisorption, which might be explained by the dilution of nickel surface by indium atoms. The lack of high temperature desorption peaks after the first CO pulse chemisorption on Ni/SiO_2 catalyst might refer to the aforementioned strong metal-support interaction between the silica and the nickel nanoparticles. Since the nickel nanoparticles are obtained from the highly dispersed, silica covered NiO particles during the first reduction, it is reasonable to suppose that these nickel nanoparticles are still partially covered by silica after the first reduction and therefore two site chemisorption of CO is hindered.

Carbon dioxide desorption was also observed on both catalysts. Carbon dioxide most likely comes from the Boudouard reaction as it was reported previously [39], [40], [42] Similarly to the CO-TPD patterns, the CO_2-TPD patterns are also quite different on the two catalysts.

The amount of CO_2 is larger on Ni/SiO_2 than on $Ni\text{-}In/SiO_2$ catalyst and only slightly decreases during the experiments. Note that in parallel with the appearance of high temperature CO desorption peaks in the CO-TPD pattern, high temperature shoulders appear in the CO_2-TPD pattern as well. This feature cannot be observed in the case of the bimetallic catalyst, the main CO desorption peak is centered at around 200 °C and there are no desorption at higher temperature. Furthermore, the amount of CO_2 is proportional to the amount of CO, as the amount of CO decreases (possibly due to particle size increase due to the repeated red-ox cycles) the amount of desorbing CO_2 also decreases. Based on the results, it can be concluded that the available active sites are very different on the two catalysts. The adsorption of CO is stronger on Ni/SiO_2 and during thermodesorption, larger portion of CO is converted to CO_2 on Ni/SiO_2 than on $Ni\text{-}In/SiO_2$ therefore it seems that the Boudouard reaction is less favored on the bimetallic catalyst.

1.2. X-ray Photoelectron Spectroscopy

To follow the changes on the catalyst surface during red-ox cycles and to describe the catalytically active sites formed after reduction, XPS measurements were conducted. The as prepared and calcined samples were stored under air before the measurements. Samples after the first TPR were exposed to air during transfer to the XPS, therefore these samples were re-reduced *in situ* at 400 °C in flowing hydrogen in a pretreatment chamber attached to our spectrometer prior to XPS measurements. After this, the samples were oxidized *in situ* in flowing air at 500 °C, which was followed by an *in situ* reduction in hydrogen flow at 500 °C. The results are summarized in Table 2, and Figure 3.

Table 2. XPS results of Ni/SiO_2 and $Ni\text{-}In/SiO_2$ catalysts after different pretreatments.

	Ni/SiO2		Ni-In/SiO2				
	Ni $2p_{3/2}$ (B.E.)	Ni/Si[a]	Ni $2p_{3/2}$ (B.E.)	Ni/Si[a]	In $3d_{5/2}$ (B.E.)	In/Si[b]	Ni/In[c]
as prepared	856.3	0.21	856.7	0.13	445.3	0.04	3.3
calc 700 °C	856.6	0.13	856.9	0.09	445.4	0.03	3.0
in situ H_2 400 °C[d]	852.4	0.04	852.3 (854.9)	0.03	444.2	0.015	2.2
in situ air 500 °C[e]	855.2	0.07	855.4	0.04	444.7	0.016	2.5
in situ H_2 500 °C[f]	852.2	0.03	852.5 (855.5)	0.03	444.3	0.012	2.5

a: peak area ratio of Ni 2p and Si 2p region.

b: peak area ratio of peaks in the In 3d and Si 2p region.

c: peak area ratio of Ni 2p and In 3d region.

d: sample in situ reduced in H_2 at 400 °C in an atmospheric pretreatment chamber attached to the spectrometer prior to measurement.

e: sample d in situ calcined in air at 500 °C in an atmospheric pretreatment chamber attached to the spectrometer prior to measurement.
f: sample e in situ reduced in H_2 at 500 °C in an atmospheric pretreatment chamber attached to the spectrometer prior to measurement.

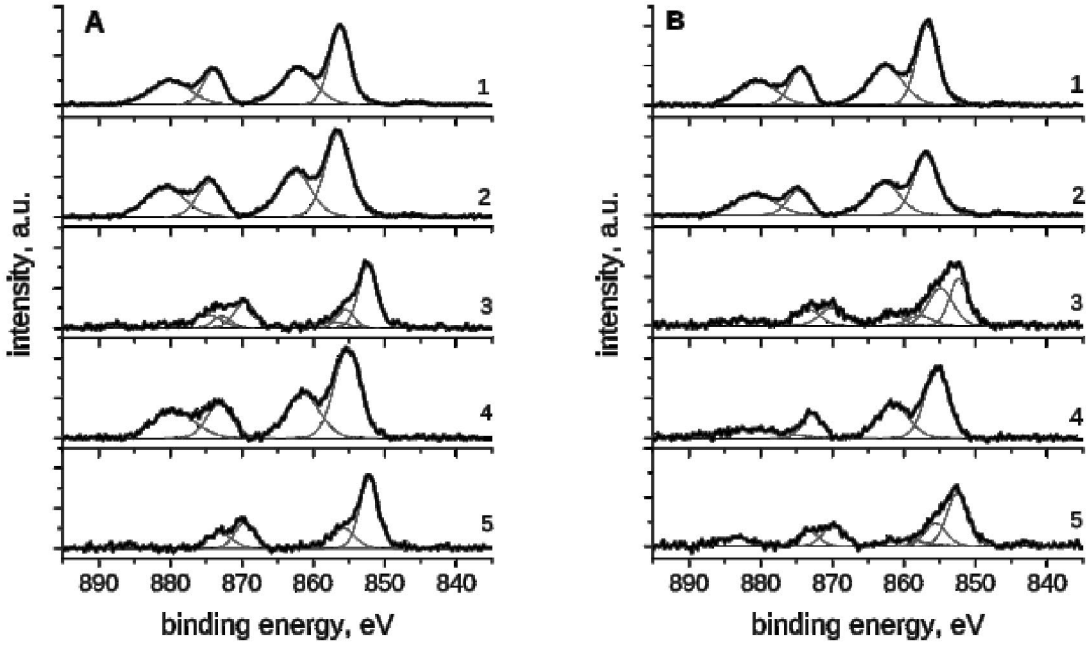

Figure 3. Ni 2p XP spectra of Ni/SiO_2 (A) and $Ni\text{-}In/SiO_2$ (B) catalysts. Spectra from top to bottom: as prepared (1); ex situ calcined at 700 °C (2); in situ reduced in H_2 at 400 °C after the first TPR (3), in situ calcined in air at 500 °C (4), in situ reduced in H_2 at 500 °C (5).

1.2.1. Chemical state of nickel on Ni/SiO_2 catalyst

Our TPR results suggest that the nickel species formed by deposition-precipitation with urea decomposes during high temperature calcination at 700 °C forming a disperse NiO phase with strong interaction to the silica support ($NiO\text{-}SiO_2$). Due to the subsequent reduction and oxidation at high temperature, this phase irreversibly transforms to silica supported nickel oxide (NiO/SiO_2) which explains the difference between the first and the second TPR curves. The XPS measurements support these findings: the binding energy of Ni $2p_{3/2}$ peak measured on the as prepared catalyst is 856.3 eV, which refers to the ionic form of nickel, most likely in the form of layered nickel silicate or nickel hydroxide (Figure 3A). After calcination this value shifts to slightly higher value, 856.6 eV, which is higher than the value corresponding to bulk NiO [43], [44]. According to the literature, this increase can be attributed to nickel oxide in strong interaction with the silica support [43]. After reduction and subsequent oxidation, the binding energy of Ni $2p_{3/2}$ is 855.2 eV which value is very close to that of bulk NiO and can be attributed to supported nickel oxide without strong interaction with the silica (NiO/SiO_2).

After *in situ* re-reduction at 400 °C, the nickel is reduced to metallic state, the binding energy of Ni $2p_{3/2}$ shifts to 852.4 eV. This sample was oxidized again *in situ* at 500 °C leading to the formation of supported nickel oxide, as it was mentioned above. This supported nickel

oxide can be fully reduced again *in situ* to supported nickel nanoparticles, the binding energy of Ni $2p_{3/2}$ photoelectron peak is shifted to 852.2 eV.

1.2.2. Chemical state of nickel and indium in the bimetallic catalysts

As it can be seen in Table 2, after catalyst preparation the binding energy of both Ni $2p_{3/2}$ and In $3d_{5/2}$ peaks is slightly higher than that of the value corresponding to bulk hydroxides. This increased binding energy of both metals might be explained by the increased hydroxide ion concentration in the close vicinity of the metal ions referring to the presence of mixed hydroxides and/or layered silicates as it was suggested previously. After calcination, the B.E. of Ni $2p_{3/2}$ peak is 856.9 eV, which is 0.3 eV higher than 856.6 eV, measured for the monometallic catalyst. Similarly, the B.E. of In $3d_{5/2}$ is 445.3 eV, slightly higher than the value corresponding to bulk In_2O_3 (444.7 eV) [45].

After *in situ* re-reduction at 400 °C, the Ni $2p_{3/2}$ peak has two spectral components, one at 852.3 eV and one at 854.9 eV. The former was identified as metallic and the latter as ionic nickel, which is quite surprising because our TPR measurements after room temperature oxidation (not shown for sake of brevity) showed that there was no H_2 consumption on the sample above 400 °C, i.e. the reduction was complete. Moreover, the slightly more oxyphilic indium is in metallic state according to the position of the In $3d_{5/2}$ peak at 444.2 eV. The appearance of metallic nickel and indium implies the intimate interaction of the metals, although the interaction is not reflected in the photoelectron peak positions.

The presence of the ionic nickel might be explained by the enrichment of indium on the surface of bimetallic nanoparticles during reduction. The TPR curves of the monometallic and bimetallic catalyst don't differ significantly, suggesting that indium oxide reduces together with nickel oxide, most likely through spillover of hydrogen from the neighboring reduced Ni sites. Reduced indium atoms from the interface of the two oxides diffuse into the Ni-NiO_x particles forming bimetallic Ni-In surface regions, which probably results in hindered diffusion of hydrogen in the metal particles, making it more difficult to reduce the NiO_x situated in the deeper surface layers. Note, that according to the TPR measurements, all of the NiO is reduced, so the amount of oxidized nickel observed by XPS is very small, almost negligible.

The enrichment of indium on the particle surface and bimetallic particle formation can be followed by the metal ratios calculated after the different treatments. To follow relative changes, the metal to Si ratios are normalized to the highest values (as prepared state) and presented in Figure 4. It can be seen, that the Ni/Si ratio obtained after the first calcination cannot be restored by subsequent red-ox cycles, which is in parallel with the results of TPR measurements and the B.E. values of the metals, and refers to the altered nickel oxide-silica interaction after the first and subsequent oxidations. The Ni/Si ratio after different pretreatments follows the same trend on the two catalysts, which means that the presence of indium on the surface does not have influence on the nickel-silica interaction.

Interestingly, the changes of In/Si ratio also follows the trend of the Ni/Si ratio. Knowing form the TPR measurements that the indium itself is weakly bonded to the silica support, the trend in the change of In/Si ratio should be different than the Ni/Si ratio without Ni-In interaction. This clearly supports the interaction of the two metals. Therefore the Ni/In ratio is the actual ratio of the metals on the surface of the bimetallic particles. After the first reduction, the Ni/In ratio is 2.2 which is lower than the nominal value of 3 (the initial Ni/In ratio was 3.3) and represents the enrichment of indium on the nickel surface. Note that after the second reduction, the ionic component of Ni $2p_{3/2}$ peak decreases while the Ni/In ratio increases to 2.5 which means that the less indium on the surface, the deeper the reduction.

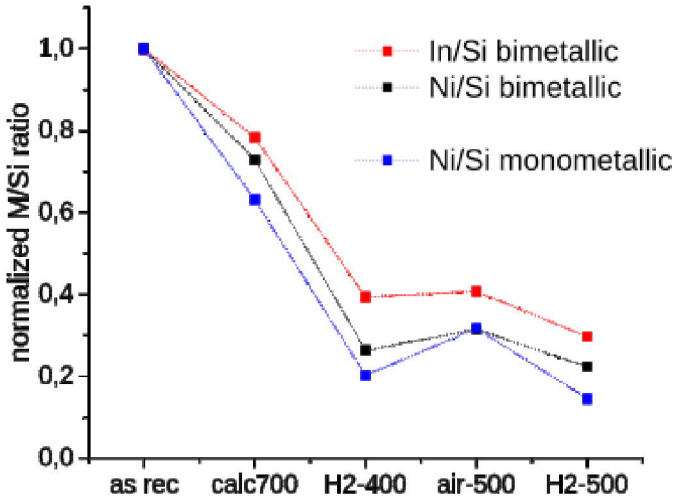

Figure 4. Relative changes of metal to silicon ratios based on photoelectron peak areas.

1.1. Catalytic tests and temperature programmed oxidation of the spent samples

1.1.1. Subsequent short catalytic cycles

The effect of indium and consecutive red-ox cycles on the catalytic performance was tested using a reactant mixture with high methane content (CH_4:CO_2:Ar = 69:30:1) at 600 °C modelling the composition of biogas [46]. Before every catalytic tests, the catalysts were calcined and reduced at 700 °C for 1 hour without removing the catalyst form the reactor. The thermal treatment following the catalytic tests was a temperature-programmed oxidation (TPO) in order to check the carbon formation tendency of the catalysts. The results of the catalytic tests and TPO curves of the monometallic and bimetallic catalyst can be seen in Figure 5 and Figure 6, respectively.

The performance of the monometallic catalyst is quite stable, it is unaffected by the subsequent catalytic cycles. The CO/H_2 ratio, which stabilizes at around 1.45 after two hours at 600 °C in each case. This value is higher than the equilibrium (CO/H_2 ~ 1.2) at this temperature [47] which usually means that some CO is produced via the reverse water-gas shift (RWGS) that is a dominant side reaction [47], [48]. TPO curves after the reaction showed that the amount of carbon deposited on the surface increased after each catalytic cycles, so it can be concluded that in our case, the coke, deposited during reaction, does not influence the catalytic activity of Ni/SiO_2 catalyst. TwoTPO peaks can be observed, one at low (300-350 °C) and one at high (600-700 °C) temperatures. The former can be assigned to the oxidation of the reactive carbon deposits in the close vicinity of nickel particles, the latter corresponds to the oxidation of polymerized carbon [49] far from active nickel sites. The intensity of the low temperature CO_2 peak does not increase, while the intensity of the high temperature peak increases significantly after each catalytic cycle. Previously, it was shown that the metal-support interaction changes after the first red-ox cycle, while the active metal surface does not change significantly (CO chemisorption results, Table 1). Based on these observations, it can be concluded that the altered metal-support interaction is responsible for the extensive carbon formation on this catalyst.

The reaction starts at higher temperatures on the bimetallic catalyst and the conversion at 600 °C slowly decreases in time, after two hours however, it is slightly higher than the values measured on the monometallic catalyst (Figure 6). The higher onset temperature might be related to the compositional changes of the bimetallic particle surface upon repeated

pretreatment and catalytic cycles as XPS results suggested. Although XPS studies showed that the amount of indium on the surface slightly decreases during these repeated red-ox cycles, it seems that the activation of reactants is still affected by the presence of indium. The measured CO/H_2 ratio (1.55-1.73) is slightly higher than that of the monometallic catalyst, which is in line with the slightly higher CO_2 conversion measured on the bimetallic catalyst, which also suggests the dominance of RWGS side reaction. Apart from these small differences, it can be concluded that the indium does not have significant influence on the overall catalytic activity of a silica supported nickel catalyst at this composition.

The most prominent difference between the two catalysts is that carbon formation was not observed on the bimetallic catalyst after the test runs (Figure 6D). The lack of coke formation can be attributed to the presence of metallic indium in the close vicinity of the nickel, which is suggested by the TPR, CO-TPD and XPS results. It is very likely that indium has the same effect as the inert modifying elements (S, Ag, Au, Sn) on nickel, that is indium changes the structure of the adsorption sites on the nickel particle, thereby limiting the methane and CO activation and/or inhibiting the diffusion and polymerization of carbon species. It has to be taken into account, that metallic indium can react not only with carbon dioxide but also with water produced in the RWGS side reaction, forming indium suboxide on the surface, which might oxidize the surface carbon formed during methane cracking and Boudouart reaction [50], [51].

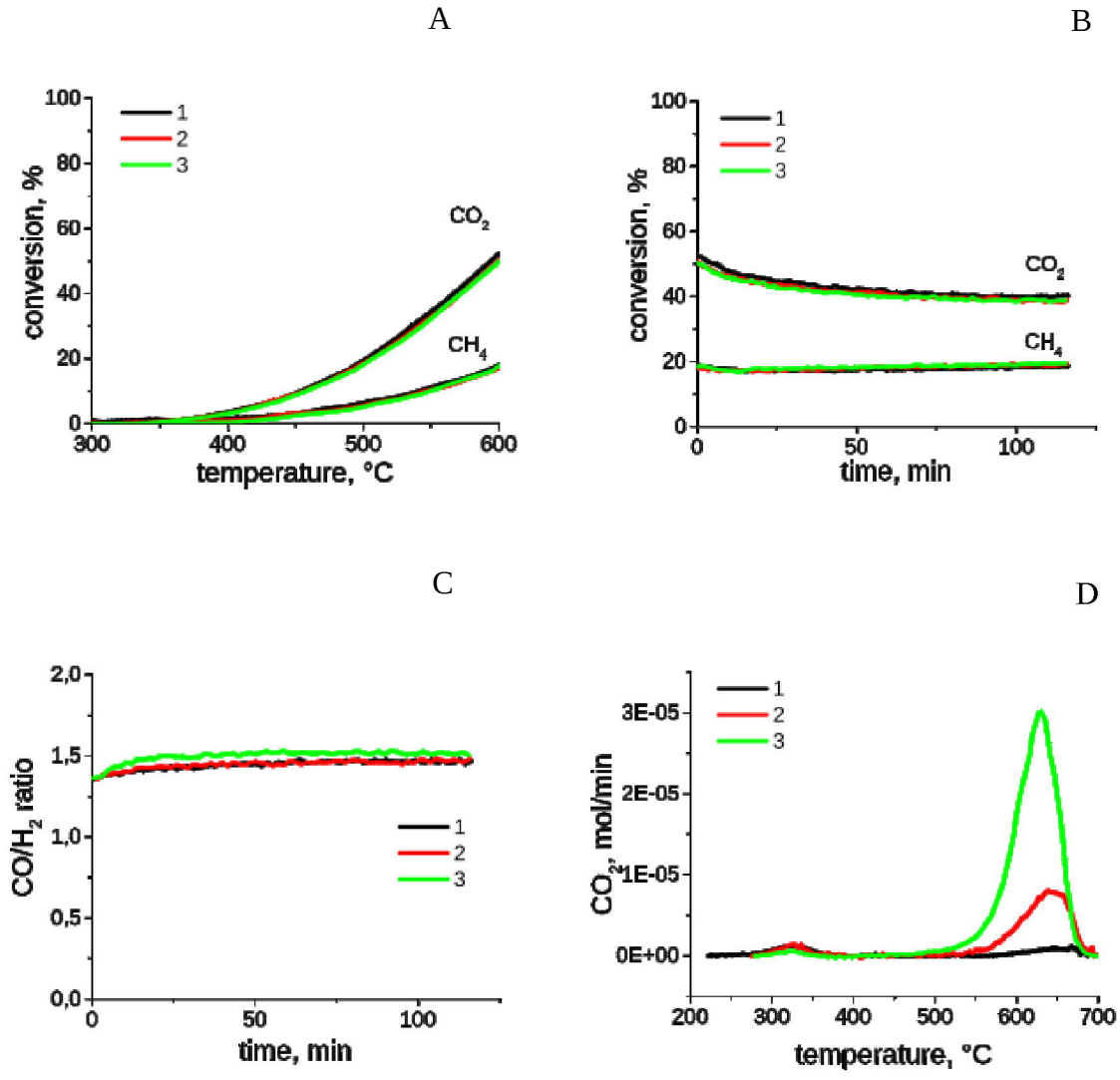

Figure 5. (A): Consecutive temperature-programmed dry reforming of methane over 3wt%Ni/SiO_2 up to 600 °C; (B): time on stream for 2 hours at 600 °C (CH_4:CO_2:Ar=69:30:1); (C): CO/H_2 ratio in the product stream during time on stream at 600 °C; (D): TPO curves obtained after each catalytic tests.

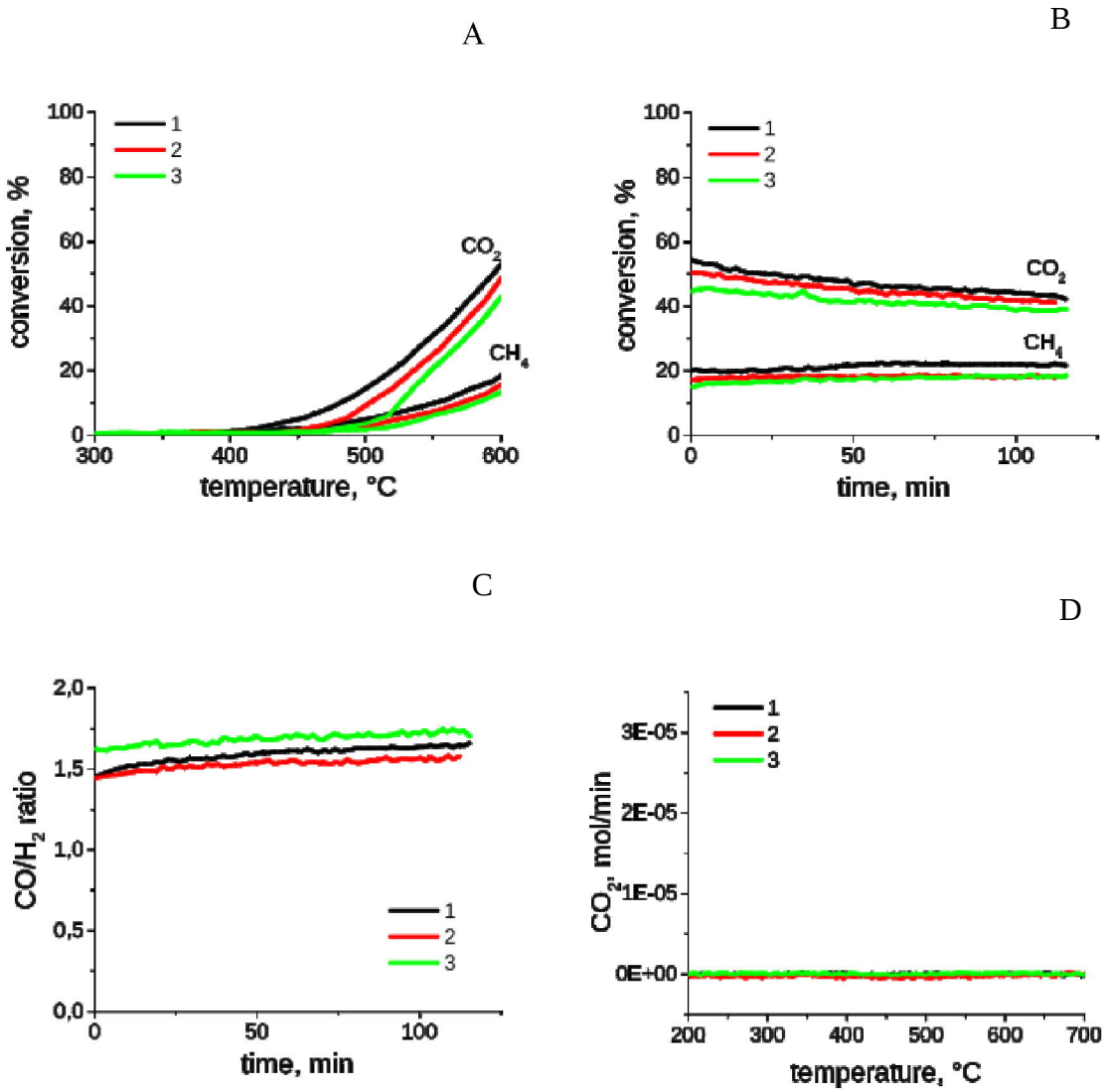

Figure 6. (A): Consecutive temperature-programmed dry reforming of methane over 3wt%Ni-2wt%In/SiO_2 up to 600 °C (CH_4:CO_2:Ar=69:30:1); (B): time on stream for 2 hours at 600 °C; (C): CO/H_2 ratio in the product stream during time on stream at 600 °C; (D): TPO curves obtained after each catalytic tests.

1.1.2. Long catalytic tests

Twenty-four hours long DRM tests at 675 °C were done to investigate the long term stability of the catalysts. The results are summarized in Figure 7. It can be seen that both of the catalysts are stable, the conversion values are higher in the case of the bimetallic catalyst. The CO/H_2 ratio stabilized at around 1.3 at this temperature on both catalysts.

Similarly to the short catalytic runs, after 24 hours' time on stream, carbon formation on the indium containing catalyst was not observed by TPO measurements (Figure 7B), while

there is a single CO_2 peak centered at 340 °C on the monometallic nickel catalyst. This is in line with the results of the first short DRM test, after which only a low temperature TPO peak at 325 °C with similar intensity was observed on the Ni/SiO_2 catalyst. This suggests that the magnitude of carbon formation on Ni/SiO_2 is independent of the time on stream of the catalyst and mostly depends on the metal-support interaction.

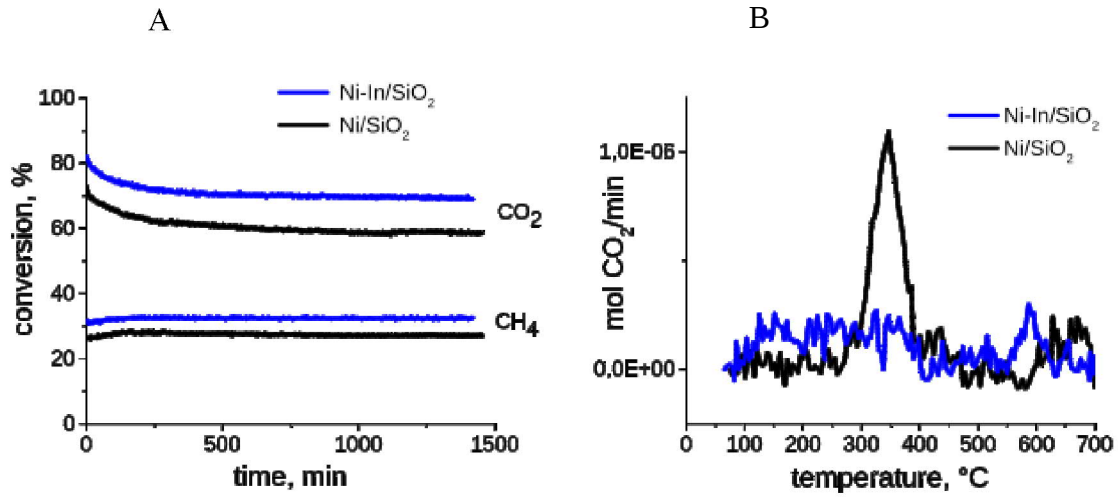

Figure 7. Long-term stability tests at 675 °C (CH_4:CO_2:Ar=69:30:1). (A): conversion curves; (B): TPO curves obtained after 24 hour reforming.

After the long catalytic tests but before the TPO, a small amount of sample was taken out of the reactor and analyzed by TEM. The results are shown in figure 8. Surprisingly, after the long catalytic test, the average particle size was quite small, 5.1 nm and 4.7 nm for the monometallic and for the bimetallic catalyst, respectively. Although the average particle size of the bimetallic catalyst is slightly smaller, it is not likely that this difference is responsible for the inhibited carbon formation.

It is worth mentioning that both average particle size is in the range when carbon formation is not expected, however coke formation occurs on Ni/SiO_2. Also, this surface carbon has absolutely no influence on the catalytic properties of the Ni/SiO_2 catalyst. Even though carbon deposits did not lead to deactivation of Ni/SiO_2 catalyst in our case, their accumulation on the longer run may cause physical blockage of reactor tubes [52].

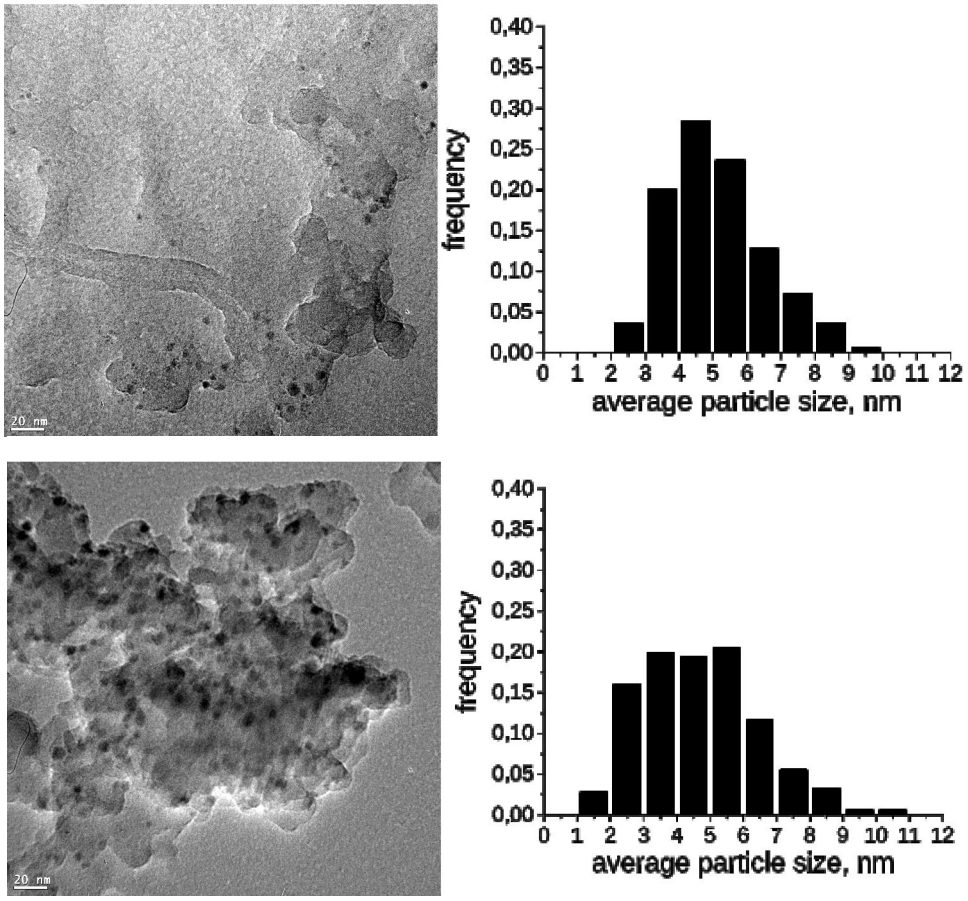

Figure 8. TEM images of the catalyst with particle size distributions after long DRM test at 675 °C. Top: 3wt%Ni/SiO_2, average particle size: 5.1 nm; Bottom: 3wt%Ni-2wt%In/SiO_2, average particle size: 4.7 nm.

2. Conclusion

It was shown that the presence of 2wt% indium on the surface of a 3wt%Ni/SiO_2 catalyst prevented coke formation during dry reforming of methane. TPR results pointed out that indium was unstable against sintering without nickel on the silica surface, however in the bimetallic catalyst it was in metallic state and mixed with nickel after reduction at 700 °C. The presence of indium profoundly changed the adsorption properties of nickel, as CO-TPD measurements suggested. XPS measurements showed changes in the electronic structure of nickel on the Ni-In/SiO_2 catalyst after reduction, moreover, they revealed the presence of bimetallic particles which surface composition found to be $Ni_{2.2}In$, lower than the expected Ni_3In, referring to indium enrichment on the surface. TEM analysis of the spent catalysts after 24 hours' time on stream showed that the average particle size of the bimetallic catalyst was slightly smaller than that of the monometallic catalyst. Based on the presented results, the higher catalytic activity and outstanding carbon tolerance of the bimetallic Ni-In/SiO_2 catalyst is the consequence of a structural and electronic effects of indium.

3. Acknowledgement

The financial support and the Postdoctoral Scholarship provided by the Hungarian National Research Fund (OTKA PD#116384) is greatly acknowledged.
The authors are also indebted for financial support of Era-Chemistry and the Hungarian National Research Fund (OTKA NN#107170).
The authors are thankful to Dr. László Kövér, Dr. József Tóth, Dr. Dávid Srankó for their help and comments concerning the XPS results. The authors are grateful to Dr. Andrea Beck for her overall comments and suggestions.

4. References

[1] R.S. Haszeldine, Carbon Capture and Storage: How Green Can Black Be?, Science. 325 (2009) 1647–1652. doi:10.1126/science.1172246.
[2] IPCC - Carbon Dioxide Capture and Storage (SRCCS), (n.d.). https://www.ipcc.ch/report/srccs/ (accessed November 7, 2016).
[3] J.S.H.Q. Perera, J.W. Couves, G. Sankar, J.M. Thomas, The catalytic activity of Ru and Ir supported on Eu2O3 for the reaction, CO2 + CH4 ⇄ 2 H2 + 2 CO: a viable solar-thermal energy system, Catal. Lett. 11 (1991) 219–225. doi:10.1007/BF00764088.
[4] S. Wang, G.Q. (Max) Lu, G.J. Millar, Carbon Dioxide Reforming of Methane To Produce Synthesis Gas over Metal-Supported Catalysts: State of the Art, Energy Fuels. 10 (1996) 896–904. doi:10.1021/ef950227t.
[5] M.-S. Fan, A.Z. Abdullah, S. Bhatia, Catalytic Technology for Carbon Dioxide Reforming of Methane to Synthesis Gas, ChemCatChem. 1 (2009) 192–208. doi:10.1002/cctc.200900025.
[6] G. Centi, S. Perathoner, Opportunities and prospects in the chemical recycling of carbon dioxide to fuels, Catal. Today. 148 (2009) 191–205. doi:10.1016/j.cattod.2009.07.075.
[7] M.C.J. Bradford, M.A. Vannice, CO2Reforming of CH4over Supported Pt Catalysts, J. Catal. 173 (1998) 157–171. doi:10.1006/jcat.1997.1910.
[8] A. Erdohelyi, J. Cserenyi, F. Solymosi, Activation of CH4 and Its Reaction with CO2 over Supported Rh Catalysts, J. Catal. 141 (1993) 287–299. doi:10.1006/jcat.1993.1136.
[9] A. Erdöhelyi, J. Cserényi, E. Papp, F. Solymosi, Catalytic reaction of methane with carbon dioxide over supported palladium, Appl. Catal. Gen. 108 (1994) 205–219. doi:10.1016/0926-860X(94)85071-2.
[10] D.L. Trimm, The Formation and Removal of Coke from Nickel Catalyst, Catal. Rev. 16 (1977) 155–189. doi:10.1080/03602457708079636.
[11] M.C.J. BRADFORD, M.A. VANNICE, CO2 Reforming of CH4, Catal. Rev. 41 (1999) 1–42. doi:10.1081/CR-100101948.
[12] D. Chen, K.O. Christensen, E. Ochoa-Fernández, Z. Yu, B. Tøtdal, N. Latorre, A. Monzón, A. Holmen, Synthesis of carbon nanofibers: effects of Ni crystal size during methane decomposition, J. Catal. 229 (2005) 82–96. doi:10.1016/j.jcat.2004.10.017.
[13] S. Tang, L. Ji, J. Lin, H.C. Zeng, K.L. Tan, K. Li, CO2 Reforming of Methane to Synthesis Gas over Sol–Gel-made Ni/γ-Al2O3 Catalysts from Organometallic Precursors, J. Catal. 194 (2000) 424–430. doi:10.1006/jcat.2000.2957.
[14] J.-H. Kim, D.J. Suh, T.-J. Park, K.-L. Kim, Effect of metal particle size on coking during CO2 reforming of CH4 over Ni–alumina aerogel catalysts, Appl. Catal. Gen. 197 (2000) 191–200. doi:10.1016/S0926-860X(99)00487-1.

[15] X. Guo, Y. Sun, Y. Yu, X. Zhu, C. Liu, Carbon formation and steam reforming of methane on silica supported nickel catalysts, Catal. Commun. 19 (2012) 61–65. doi:10.1016/j.catcom.2011.12.031.
[16] T.D. Gould, A. Izar, A.W. Weimer, J.L. Falconer, J.W. Medlin, Stabilizing Ni Catalysts by Molecular Layer Deposition for Harsh, Dry Reforming Conditions, ACS Catal. 4 (2014) 2714–2717. doi:10.1021/cs500809w.
[17] Z. Li, L. Mo, Y. Kathiraser, S. Kawi, Yolk–Satellite–Shell Structured Ni–Yolk@Ni@SiO2 Nanocomposite: Superb Catalyst toward Methane CO2 Reforming Reaction, ACS Catal. 4 (2014) 1526–1536. doi:10.1021/cs401027p.
[18] E. Ruckenstein, Y. Hang Hu, Role of Support in CO2Reforming of CH4to Syngas over Ni Catalysts, J. Catal. 162 (1996) 230–238. doi:10.1006/jcat.1996.0280.
[19] T. Horiuchi, K. Sakuma, T. Fukui, Y. Kubo, T. Osaki, T. Mori, Suppression of carbon deposition in the CO2-reforming of CH4 by adding basic metal oxides to a Ni/Al2O3 catalyst, Appl. Catal. Gen. 144 (1996) 111–120. doi:10.1016/0926-860X(96)00100-7.
[20] Y. Pan, P. Kuai, Y. Liu, Q. Ge, C. Liu, Promotion effects of Ga2O3 on CO2 adsorption and conversion over a SiO2-supported Ni catalyst, Energy Environ. Sci. 3 (2010) 1322–1325. doi:10.1039/C0EE00149J.
[21] K.Y. Koo, H.-S. Roh, U.H. Jung, W.L. Yoon, CeO2 Promoted Ni/Al2O3 Catalyst in Combined Steam and Carbon Dioxide Reforming of Methane for Gas to Liquid (GTL) Process, Catal. Lett. 130 (2009) 217. doi:10.1007/s10562-009-9867-4.
[22] X. Zhu, P. Huo, Y. Zhang, D. Cheng, C. Liu, Structure and reactivity of plasma treated Ni/Al2O3 catalyst for CO2 reforming of methane, Appl. Catal. B Environ. 81 (2008) 132–140. doi:10.1016/j.apcatb.2007.11.042.
[23] I. Alstrup, A new model explaining carbon filament growth on nickel, iron, and NiCu alloy catalysts, J. Catal. 109 (1 988) 241–251. doi:10.1016/0021-9517(88)90207-2.
[24] M. Araki, V. Ponec, Methanation of carbon monoxide on nickel and nickel-copper alloys, J. Catal. 44 (1976) 439–448. doi:10.1016/0021-9517(76)90421-8.
[25] W.L. van Dijk, J.A. Groenewegen, V. Ponec, The dissociative adsorption of CO on nickel and nickel-copper alloys, J. Catal. 45 (1976) 277–280. doi:10.1016/0021-9517(76)90144-5.
[26] W. Erley, H. Wagner, Sulfur poisoning of carbon monoxide adsorption on Ni(111), J. Catal. 53 (1978) 287–294. doi:10.1016/0021-9517(78)90101-X.
[27] N.V. Parizotto, K.O. Rocha, S. Damyanova, F.B. Passos, D. Zanchet, C.M.P. Marques, J.M.C. Bueno, Alumina-supported Ni catalysts modified with silver for the steam reforming of methane: Effect of Ag on the control of coke formation, Appl. Catal. Gen. 330 (2007) 12–22. doi:10.1016/j.apcata.2007.06.022.
[28] A. Horváth, L. Guczi, A. Kocsonya, G. Sáfrán, V. La Parola, L.F. Liotta, G. Pantaleo, A.M. Venezia, Sol-derived AuNi/MgAl2O4 catalysts: Formation, structure and activity in dry reforming of methane, Appl. Catal. Gen. 468 (2013) 250–259. doi:10.1016/j.apcata.2013.08.053.
[29] H.S. Bengaard, J.K. Nørskov, J. Sehested, B.S. Clausen, L.P. Nielsen, A.M. Molenbroek, J.R. Rostrup-Nielsen, Steam Reforming and Graphite Formation on Ni Catalysts, J. Catal. 209 (2002) 365–384. doi:10.1006/jcat.2002.3579.
[30] A. Fouskas, M. Kollia, A. Kambolis, C. Papadopoulou, H. Matralis, Boron-modified Ni/Al2O3 catalysts for reduced carbon deposition during dry reforming of methane, Appl. Catal. Gen. 474 (2014) 125–134. doi:10.1016/j.apcata.2013.08.016.
[31] J. Xu, M. Saeys, Improving the coking resistance of Ni-based catalysts by promotion with subsurface boron, J. Catal. 242 (2006) 217–226. doi:10.1016/j.jcat.2006.05.029.

[32] E. Nikolla, A. Holewinski, J. Schwank, S. Linic, Controlling Carbon Surface Chemistry by Alloying: Carbon Tolerant Reforming Catalyst, J. Am. Chem. Soc. 128 (2006) 11354–11355. doi:10.1021/ja0638298.
[33] N.N. Nichio, M.L. Casella, G.F. Santori, E.N. Ponzi, O.A. Ferretti, Stability promotion of Ni/α-Al2O3 catalysts by tin added via surface organometallic chemistry on metals: Application in methane reforming processes, Catal. Today. 62 (2000) 231–240. doi:10.1016/S0920-5861(00)00424-7.
[34] Z. Hou, O. Yokota, T. Tanaka, T. Yashima, Surface properties of a coke-free Sn doped nickel catalyst for the CO2 reforming of methane, Appl. Surf. Sci. 233 (2004) 58–68. doi:10.1016/j.apsusc.2004.03.223.
[35] P. Sun, G. Siddiqi, W.C. Vining, M. Chi, A.T. Bell, Novel Pt/Mg(In)(Al)O catalysts for ethane and propane dehydrogenation, J. Catal. 282 (2011) 165–174. doi:10.1016/j.jcat.2011.06.008.
[36] D. Baudouin, U. Rodemerck, F. Krumeich, A. de Mallmann, K.C. Szeto, H. Ménard, L. Veyre, J.-P. Candy, P.B. Webb, C. Thieuleux, C. Copéret, Particle size effect in the low temperature reforming of methane by carbon dioxide on silica-supported Ni nanoparticles, J. Catal. 297 (2013) 27–34. doi:10.1016/j.jcat.2012.09.011.
[37] P. Burattin, M. Che, C. Louis, Characterization of the Ni(II) Phase Formed on Silica Upon Deposition−Precipitation, J. Phys. Chem. B. 101 (1997) 7060–7074. doi:10.1021/jp970194d.
[38] O. Clause, L. Bonneviot, M. Che, Effect of the preparation method on the thermal stability of silica-supported nickel oxide as studied by EXAFS and TPR techniques, J. Catal. 138 (1992) 195–205. doi:10.1016/0021-9517(92)90017-C.
[39] J.L. Falconer, A.E. Zağli, Adsorption and methanation of carbon dioxide on a nickel/silica catalyst, J. Catal. 62 (1980) 280–285. doi:10.1016/0021-9517(80)90456-X.
[40] A. Tanksale, J.N. Beltramini, J.A. Dumesic, G.Q. Lu, Effect of Pt and Pd promoter on Ni supported catalysts—A TPR/TPO/TPD and microcalorimetry study, J. Catal. 258 (2008) 366–377. doi:10.1016/j.jcat.2008.06.024.
[41] P.A. Redhead, Chemisorption on polycrystalline tungsten. Part 1.—Carbon monoxide, Trans. Faraday Soc. 57 (1961) 641–656. doi:10.1039/TF9615700641.
[42] M.W. Balakos, S.S.C. Chuang, CO disproportionation on Ni-based catalysts, React. Kinet. Catal. Lett. 49 (1993) 7–12. doi:10.1007/BF02084022.
[43] J.C. Vedrine, G. Hollinger, Tran Minh Duc, Investigations of antigorite and nickel supported catalysts by x-ray photoelectron spectroscopy, J. Phys. Chem. 82 (1978) 1515–1520. doi:10.1021/j100502a011.
[44] P. Lorenz, J. Finster, G. Wendt, J.V. Salyn, E.K. Žumadilov, V.I. Nefedov, Esca investigations of some NiO/SiO2 and NiO—Al2 O3 /SiO2 catalysts, J. Electron Spectrosc. Relat. Phenom. 16 (1979) 267–276. doi:10.1016/0368-2048(79)80023-7.
[45] M. Faur, M. Faur, D.T. Jayne, M. Goradia, C. Goradia, XPS investigation of anodic oxides grown on p-type InP, Surf. Interface Anal. 15 (1990) 641–650. doi:10.1002/sia.740151102.
[46] S.E. Evans, J.Z. Staniforth, R.J. Darton, R.M. Ormerod, A nickel doped perovskite catalyst for reforming methane rich biogas with minimal carbon deposition, Green Chem. 16 (2014) 4587–4594. doi:10.1039/C4GC00782D.
[47] M. Németh, Z. Schay, D. Srankó, J. Károlyi, G. Sáfrán, I. Sajó, A. Horváth, Impregnated Ni/ZrO2 and Pt/ZrO2 catalysts in dry reforming of methane: Activity tests in excess methane and mechanistic studies with labeled 13CO2, Appl. Catal. Gen. 504 (2015) 608–620. doi:10.1016/j.apcata.2015.04.006.
[48] D. Pakhare, J. Spivey, A review of dry (CO2) reforming of methane over noble metal catalysts, Chem. Soc. Rev. (2014). doi:10.1039/C3CS60395D.

[49] M.D. Argyle, C.H. Bartholomew, Heterogeneous Catalyst Deactivation and Regeneration: A Review, Catalysts. 5 (2015) 145–269. doi:10.3390/catal5010145.
[50] K. Otsuka, T. Yasui, A. Morikawa, Production of CO from CO2 by reduced indium oxide, J. Chem. Soc. Faraday Trans. 1 Phys. Chem. Condens. Phases. 78 (1982) 3281–3286. doi:10.1039/F19827803281.
[51] K. Otsuka, T. Yasui, A. Morikawa, The Decomposition of Water on the CO- or H_2 -reduced Indium Oxide, Bull. Chem. Soc. Jpn. 55 (1982) 1768–1771. doi:10.1246/bcsj.55.1768.
[52] J.R. Rostrup-Nielsen, Industrial relevance of coking, Catal. Today. 37 (1997) 225–232. doi:10.1016/S0920-5861(97)00016-3.